VNU Journal of Science: Mathematics – Physics, Vol. 41, No. 1 (2025) 26-33

VNU Journal of Science: Mathematics - Physics

Journal homepage: https://js.vnu.edu.vn/MaP

Original Article

Structure and Density Heterogeneities of the *l*-$3Al_2O_3.2SiO_2$ System: Insight from Computer Simulation and Density-Based Spatial Clustering of Applications with Noise

Mai Thi Lan, Pham Tri Dung*, Nguyen Van Hong

Hanoi University of Science and Technology, 1 Dai Co Viet, Hai Ba Trung, Hanoi, Vietnam

Received 24th September 2024
Revised 31st October 2024; Accepted 15th February 2025

Abstract: The structural and density heterogeneity of the liquid $3Al_2O_3.2SiO_2$ (l-$3Al_2O_3.2SiO_2$) system was studied using Molecular Dynamics (MD) and Monte Carlo (MC) simulations. The results showed that the structural phase transition occurred at an oxygen packing factor of approximately 0.58. At low pressure, TO_4 structural units predominated while at high pressure, TO_6 structural units became dominant. In addition, the Density-Based Spatial Clustering of Applications with Noise (DBSCAN) algorithm was applied to find regions with larger density than the average density in the model. These findings provide an in-depth understanding of the structure of the l-$3Al_2O_3.2SiO_2$ system under compressive pressure.

Keywords: Structural heterogeneity, OPF, high-density regions, DBSCAN.

1. Introduction

In recent years, Al_2O_3 and SiO_2 oxide systems have received significant research attention. $Al_2O_3.SiO_2$ system with the Al_2O_3 content at 60 mol % ($3Al_2O_3.2SiO_2$) is considered a potential material for modern ceramic production. With preeminent properties such as mechanical strength, high thermal shock resistance, low thermal expansion, and good conductivity, $3Al_2O_3.2SiO_2$ systems are widely used in electronic and optical applications [1]. Research results on the $Al_2O_3.SiO_2$ system indicate that, in the aluminosilicate glass system, both SiO_2 and Al_2O_3 serve as network formers [2]. The Si^{4+} ion preferentially combines with O^{2-} to form a glass lattice framework shaped like a tetrahedron (SiO_4). Al_2O_3 acts as a network intermediate and is an important chemical component of glass. This enhances

* Corresponding author.
E-mail address: tridungmta143@gmail.com

https//doi.org/10.25073/2588-1124/vnumap.4967

the mechanical strength and thermal stability of the materials [3-5]. Al_2O_3 has two structural forms: octahedral AlO_6 and tetrahedral AlO_4 units, which perform different functions. Notably, AlO_4 units typically make up a larger proportion. When the concentration of Al_2O_3 in the $Al_2O_3.SiO_2$ system increases, the proportion of octahedral AlO_6 also rises. The overall bonding within the glass network weakens, leading to an increase in the thermal expansion coefficient and a decrease in chemical stability. When Al_2O_3 content exceeds 6%, its role in providing free oxygen becomes prominent, which can damage the Si–O network to a certain extent [6, 7]. There have been many studies on the $Al_2O_3.SiO_2$ systems, with most focusing on the relationship between structure, temperature, and composition [8-11]. Simulation studies [12-15] have focused on studying the spatial distribution of the basic structural units TO_n as well as determining the ratios of bridging oxygen (BO) to non-bridging oxygen (NBO) in $Al_2O_3.SiO_2$. They provide valuable insights into the structure of the $Al_2O_3.SiO_2$ system.

In this work, we studied the $l\text{-}3Al_2O_3.2SiO_2$ system at 3.500 K under pressure conditions ranging from 0 to 80 GPa. We survey the bond length of atom pairs, coordination number (CN), density, and oxygen packing factor (OPF) to extract valuable structural information. In particular, the Density-Based Spatial Clustering of Applications with Noise (DBSCAN) algorithm is applied to find high-density regions to clarify the structural heterogeneity of the model. The results contributed important insights into the structural heterogeneity of the $l\text{-}3Al_2O_3.2SiO_2$.

2. Computational Procedure

The models for a $l\text{-}3Al_2O_3.2SiO_2$ system were built using MD simulation method with the Born–Mayer–Huggins potential and periodic boundary conditions. These issues are described in detail in our previous work [16]. Now, we present more information about the MC and DBSCAN methods used in this work. The MC algorithm is applied to calculate the OPF and the volume of dense clusters in the model. The algorithm's steps are as follows: 10^6 random points are placed in the MD simulation box. Based on the radius of the atoms in the model, each point is checked to determine whether it belongs to the region occupied by any atom. N_P is the number of random points in the high-density region where the atoms occupy, the volume of the simulation box is V_0. The volume of the high-density clusters (V_C) is calculated as follows:

$$V_C = \frac{N_P V_0}{10^6} \tag{1}$$

The atomic density of clusters in the high-density regions (HDR) is calculated by formula (2):

$$density = \frac{m_{Si}n_{Si}+m_O n_O+m_{Al}n_{Al}}{V_C.N_A} \tag{2}$$

where m_{Si}, n_{Si}, m_{Al}, n_{Al}, m_O, and n_O are the mass and number of Si, Al, and O atoms in the high-density clusters, respectively. N_A is Avogadro's constant.

To determine OPF, we calculate the number of points within the radius of the atoms. If N_0 is the total number of points located in the space of oxygen atoms, then OPF can be calculated, it is as follows $OPF = N_0/1{,}000{,}000$.

For the DBSCAN algorithm, it is necessary to determine the parameters appropriately for each specific data set, depending on the characteristics and nature of the data set's distribution. Two parameters needed to be selected in DBSCAN are epsilon (*eps*) and *Minpts* [17, 18]. Where *Minpts* is a threshold of the minimum number of data points grouped to define a high-density neighborhood, *eps* is the distance value used to define the neighborhood of any atom. Two parameters *eps* and *Minpts* help define three types of points: core point, border point, and noise point (noise). The steps of the algorithm are as follows:

- The algorithm selects any data point and then proceeds to determine the core and boundary points through the *eps* neighborhood by spreading the chain of points belonging to the same cluster.
- The cluster is completely defined when it cannot be expanded further. Then recursively repeat the entire process with an initial point among the remaining data points to determine a new cluster.
- Points that are not within the *eps* distance of any core point are considered as noise points, these points are not assigned to any cluster.

3. Results and Discussion

The first maximum peak of the radial distribution function (r_{max}) is shown in Fig. 1. At ambient pressure, the bond lengths of Si – Si, Si – O, O – O, Si – Al, O – Al, and Al – Al are 3.12 Å, 1.58 Å, 2.72 Å, 3.1 Å, 1.66 Å, 3.16 Å, respectively. When increasing the compression pressure, the r_{max} of the Si – O and Al – O pairs increase, this shows the growth of the Si–O and Al–O coordination number when applying pressure increase. In contrast, the r_{max} of the O–O pair decreases, more notably the bond lengths of Si–Si, Al–Al, and Si–Al atomic pairs tend to increase when the pressure increases from 0 to 6 GPa after that begin to decrease. At 80 GPa, the bond lengths of the Si–Si, Al–Al, and Si–Al pairs are 3.08 Å, 2.9 Å, and 2.96 Å, respectively. These results are consistent with the data of the simulation and experimental studies as shown in [12, 19, 20], see in Table 1.

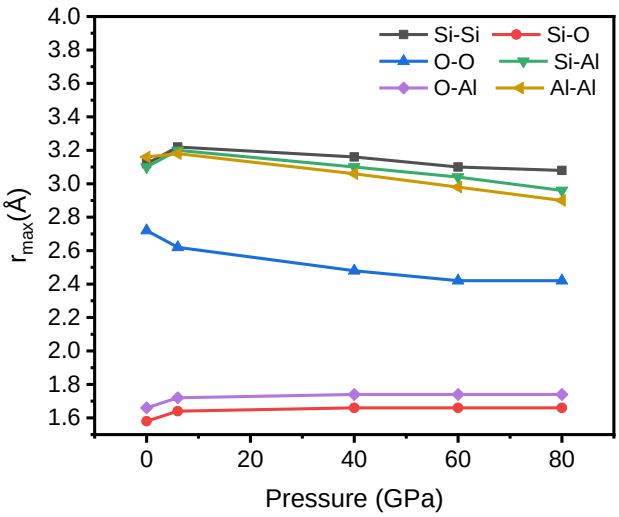

Figure 1. The r_{max} of the radial distribution functions in l-$3Al_2O_3.2SiO_2$.

Table 1. The first peak position of radial distribution functions in l-$3Al_2O_3.2SiO_2$

Fist peak position (Å)	Si-O	Al-O
This work	1.64 ± 0.02	1.72 ± 0.02
[12]	1.64	1.70
[19]	1.64	1.69
[20]	1.61	1.74

The results of the Si - O coordination number distribution are depicted in Fig. 2. It can be seen that at ambient pressure, almost one Si atom bonds with 4 oxygen atoms to form a SiO_4 polyhedron. Meanwhile the percentage of structural unit SiO_5 at this pressure is very low about 5%, and no SiO_6 unit

exists. As the pressure increases, the fraction of SiO_5 and SiO_6 increases significantly, especially from a pressure of 6 GPa, 38.56% for SiO_5 and 51.83% for SiO_6, while the proportion of SiO_4 structural units decreases sharply.

The Al–O coordination number is illustrated in Fig. 3. At ambient pressure, most of the system is AlO_4 structural units, about 68.07 %. From pressure 6 GPa, the proportion of AlO_4 decreases sharply and AlO_6 increases. At a pressure of 80 GPa, the AlO_4 structural units no longer appear, the ratio of AlO_6 units accounts for the largest ratio at 77.66 %. This result shows the structural transition from a tetrahedral to an octahedral network.

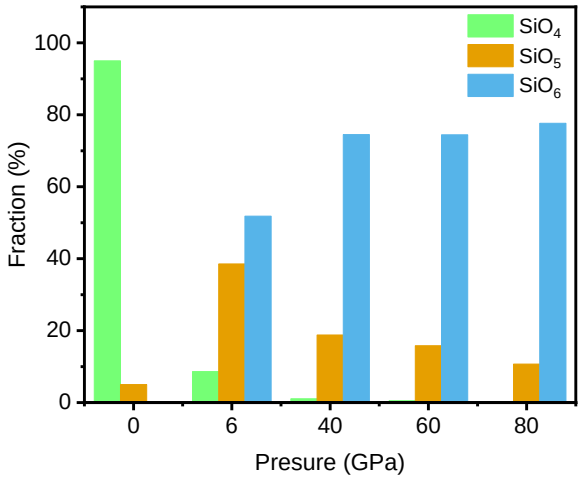

Figure 2. Coordination number distribution of Si-O pairs in l-$3Al_2O_3.2SiO_2$.

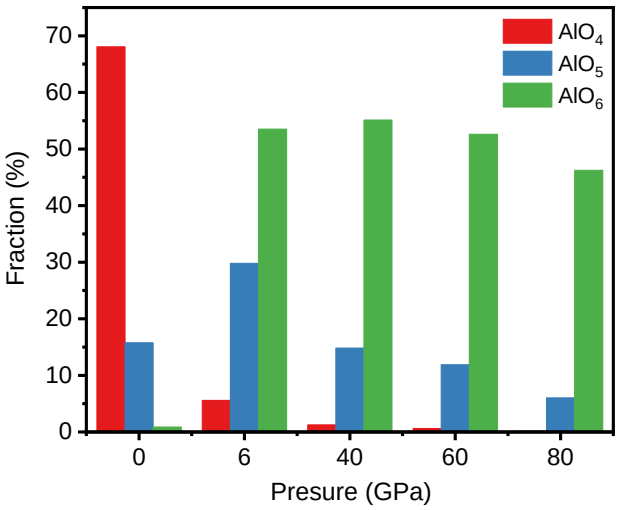

Figure 3. Coordination number distribution of Al-O pairs in l-$3Al_2O_3.2SiO_2$.

The change in the density of atoms in the *l-3Al₂O₃.2SiO₂* system from 0 GPa to 80 GPa pressure is shown in Table 2. When the pressure increases, the *l-3Al₂O₃.2SiO₂* model has a structural phase transition from the low-density phase of 2.29 g/cm^3 at 0 GPa to a high-density phase of 4.45 g/cm^3 at 80 GPa. Particularly, the density in the model changes rapidly from 2.29 g/cm^3 to 3.61 g/cm^3 at 6 GPa.

Table 2. The change of density as a function of pressure

P (GPa)	0	6	40	60	80
Density (g/cm^3)	2.29	3.61	4.05	4.25	4.45

The structural phase transition leads to a change in the OPF in the model. The OPF results are calculated and shown in Table 3. It can be seen that OPF increases with compression pressure from 0.42 at 0 GPa to 0.58 at 80 GPa, a clear change in OPF at the point pressure 6 GPa. This indicates that 6 GPa is the pressure at which the *l-3*Al_2O_3*.2*SiO_2 system undergoes a phase transition from a low-density phase to a high-density phase. The structural phase transition point corresponds to OPF = 0.58.

Table 3. The change of OPF as a function of pressure

P (Gpa)	0	6	40	60	80
OPF	0.42	0.58	0.57	0.55	0.58

To clarify the heterogeneity of the structure and density of the system, we utilize data mining to identify high-density regions at the phase transition point of 6 GPa. The atomic coordinate data is input into the Agglomerative Hierarchical Clustering (AHC) algorithm to analyze the formation of clusters within the model. In the AHC algorithm, each data point begins as an individual cluster. These clusters are then progressively merged to form larger clusters, continuing until all points in the dataset are combined into a single large cluster that encompasses the entire data set [21-24]. The clustering results are visualized using a dendrogram. In this diagram, the horizontal axis represents the index order of the observations in the original dataset, while the vertical axis indicates the dissimilarity between the clusters. A higher value on the vertical axis signifies greater dissimilarity between the represented clusters. By drawing a horizontal line that corresponds to the degree of cluster differentiation, we can count the number of intersections between this line and the vertical lines in the diagram to determine how many distinct clusters are formed [23]. From the dendrogram, it is evident that the *l-3*Al_2O_3*.2*SiO_2 system can be divided into clusters based on this differentiation criterion.

The Silhouette index is used to determine the optimal number of clusters. In Fig. 6, the Silhouette index shows the highest score for 2 clusters, indicating that the system can be divided into two clusters. In this study, we utilized the DBSCAN algorithm to divide the system into two regions: the low-density region (LDR) and the high-density region (HDR).

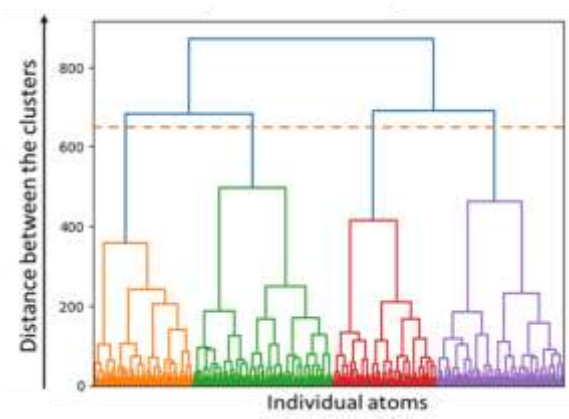

Figure 5. Dendrogram obtained from a hierarchical clustering method.

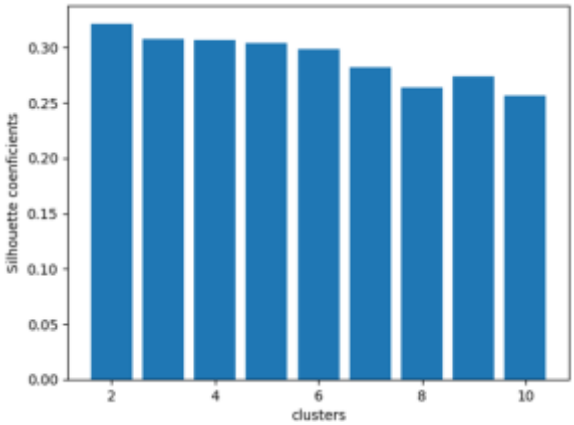

Figure 6. Silhouette coefcients as a function of clusters.

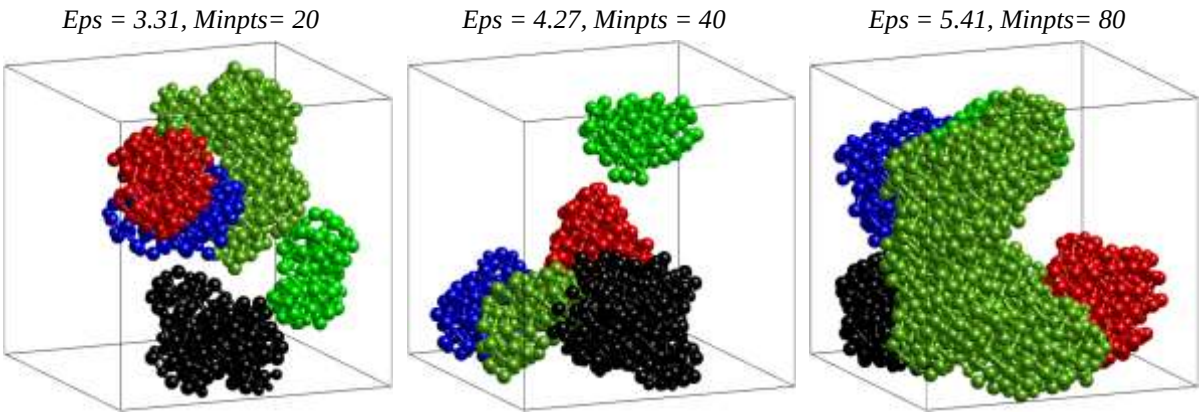

Figure 7. Top 5 clusters in HDR are highlighted in the l-$3Al_2O_3.2SiO_2$ model at 6Gpa.

Table 4. The density of atoms in high-density regions

Eps	3.31	4.28	5.41
Minpts	20	40	80
Density of clusters (g/cm^3)	20.30	21.10	21.14
Density of the model (g/cm^3)	3.61	3.61	3.61

The results demonstrate that there are clusters with densities five to six times higher than the average density of the entire model in the *l-$3Al_2O_3.2SiO_2$* system, as shown in Table 4. The size and number of atoms in the clusters depend on the parameters *eps* and *Minpts*. Figure 7 depicts the top 5 HDR in the model corresponding to parameters of the DBSCAN algorithm. This indicates the presence of structural heterogeneity in the l-$3Al_2O_3.2SiO_2$ system.

4. Conclusion

By using Molecular Dynamics and Monte Carlo simulations, along with the application of the DBSCAN data mining algorithm, we have clarified the structural characteristics and density heterogeneity of the *l-$3Al_2O_3.2SiO_2$* system under compression. Our key findings indicate that a

structural phase transition occurs at an oxygen packing fraction of approximately 0.58. By optimizing the parameters of the DBSCAN algorithm, we identified high-density regions within the model at the phase transition point. The observed polyamorphism and density heterogeneity provide valuable insights into the fundamental structural changes and compositional fluctuations that occur in this system when subjected to compression.

Acknowledgments

This research is funded by Hanoi University of Science and Technology (HUST) under project number T2024-PC-012.

References

[1] I. A. Aksay, D. M. Dabbs, M. Sarikaya, Mullite for Structural, Electronic, and Optical Applications, Journal of the American Ceramic Society, Vol. 74, 1991, pp. 2343-2358, https://doi.org/10.1111/j.1151-2916.1991.tb06768.x.

[2] S. Takahashi, D. R. Neuville, H. Takebe, Thermal Properties, Density and Structure of Percalcic and Peraluminus $CaO–Al_2O_3–SiO_2$ Glasses, Journal of Non-Crystalline Solids, Vol. 411, 2015, pp. 5-12, https://doi.org/10.1016/j.jnoncrysol.2014.12.019.

[3] K. Junfeng, C. Junzhu, L. Sheng et al., Structure, Dielectric Property and Viscosity of Alkali-Free Boroaluminosilicate Glasses with the Substitution of Al2O3 for SiO2, Journal of Non-Crystalline Solids, Journal of Non-Crystalline Solids, Vol. 537, 2020, pp. 120022, https://doi.org/10.1016/j.jnoncrysol.2020.120022.

[4] S. H. Garofalini, Molecular Dynamics Simulations of Silicate Glasses and Glass Surfaces: Applications in the Geosciences, Rev. Mineral.Geochem, Vol. 42, 2011, pp. 131-168, http://dx.doi.org/10.1515/9781501508721-008.

[5] P. F. Becher, S. Hampshire, M. J. Pomeroy et al., An Overview of the Structure and Properties of Silicon-Based Oxynitride Glasses, International Journal of Applied Glass Science, Vol. 2, 2011, pp. 63-83, https://doi.org/10.1111/j.2041-1294.2011.00042.x.

[6] X. Lin, Z. Wang, X. Jiang at el., Effect of Al_2O_3/SiO_2 Mass Ratio on the Structure and Properties of Medical Neutral Boroaluminosilicate Glass Based on XPS and Infrared Analysis, Ceramics International, Vol. 49, 2023, pp. 38499, https://doi.org/10.1016/j.ceramint.2023.09.180.

[7] C. Ji, L. Li, W. Gao, J. Wang, J. Han, Influence of Al_2O_3/SiO_2 Ratio in Multicomponent LNAS Glasses and Glass-ceramics on the Crystallization Behavior, Microstructure and Mechanical Performance, Ceramics International, Vol. 49, 2023, pp. 10652, https://doi.org/10.1016/j.ceramint.2022.11.253.

[8] H. P. A. Alves, Processing of Mullite–Glass Ceramics Using Simplex-Centroid Design: Densification Process Dominated By Liquid-Phase Sintering, Boletín De La Sociedad Española De Cerámica y Vidrio, Vol. 61, 2022, pp. 160-168, https://doi.org/10.1016/j.bsecv.2020.09.002.

[9] M. Kriven, J. W. Palko, S. Sinogeikin, J. D. Bass, A. Sayir, G. Brunauer, H. Boysen, F. Freyd, J. Schneider, High Temperature Single Crystal Properties of Mullite, J. Eur. Ceram. Soc., Vol. 19, 1999, pp. 2529, https://doi.org/10.1016/S0955-2219(99)00124-7.

[10] S. Hartmut, Mullite: Crystal Structure and Related Properties, J. Am. Ceram. Soc., Vol. 98, 2015, pp. 2948, https://doi.org/10.1111/jace.13817.

[11] M. Daniele, S. Ronchetti, A. Costanzo, Atomistic Simulations on Mullite $Al_2(Al_{2+2x}Si_{2-2x})O_{10-x}$ in a Variable Range of Composition, J. Eur. Ceram. Soc, Vol. 28, 2008, pp. 367, https://doi.org/10.1016/j.jeurceramsoc.2007.03.003.

[12] M. Benoit, S. Ispas, Structural Properties of Molten Silicates from Ab Initio Molecular-Dynamics Simulations: Comparison between $CaO-Al_2O_3-SiO_2$ and SiO_2, Physical Review B, Vol. 64, 2001, pp. 224205, https://10.1103/PhysRevB.64.224205.

[13] A. Winkler, J. Horbach, W. Kob et al., Structure and Diffusion in Amorphous Aluminum Silicate: A Molecular Dynamics Computer Simulation, J Chem Phys, Vol. 120, 2004, pp. 384, https://doi.org/10.1063/1.1630562.

[14] N. V. Yen, M. T. Lan, L. T. Vinh, N. V. Hong, Structural Properties of Liquid Aluminosilicate with Varying Al_2O_3/ SiO_2 Ratios: Insight From Analysis And Visualization of Molecular Dynamics Data, Modern Physics Letters B, Vol. 31, 2017, pp. 36, https://doi.org/10.1142/S0217984917500361.

[15] J. R. Allwardt, J. F. Stebbins, B. C. Schmidt et al., Aluminum Coordination and the Densification of High-Pressure Aluminosilicate Glasses, Am Mineralogist, Vol. 90, 2005, pp. 1218.

[16] M. T. Lan, T. Iitakay, N. V. Hong, International Journal of Modern Physics B Vol. 32, No. 24, 2018, pp. 1850271, https://doi.org/10.1142/S0217979218502715.

[17] A. L. Pakdehi, N. Daneshpour, DBHC: A DBSCAN-based Hierarchical Clustering Algorithm, Data & Knowledge Engineering, Vol. 135, 2021, pp. 101922, https://doi.org/10.1016/j.datak.2021.101922.

[18] J. Han, J. Pei, M. Kamber, Data Mining: Concepts and Techniques, Elsevier, 2011.

[19] V. E. Sokol'skii, V. Pruttskov, O. M. Yakovenko, V. P. Kazimirov, O. S. Roik, N. V. Golovataya, G. V. Sokolsky, X-ray Diffraction Study of Structure of CaO-Al_2O_3-SiO_2 Ternary Compounds in Molten and Crystalline States, J. Min. Metall. Sect. B-Metall., Vol. 56, 2020, pp. 269-277.

[20] M. Okuno, N. Zotov, M. Schmu¨cker, H. Schneider, Structure of SiO_2–Al_2O_3 Glasses: Combined X-ray Diffraction, IR and Raman Studies, Journal of Non-Crystalline Solids, Vol. 351, 2005, pp. 1032-1038.

[21] Q. Huang, R. Gao, H. Akhavan, An Ensemble Hierarchical Clustering Algorithm Based on Merits at Cluster and Partition Levels, Pattern Recogn, Vol. 136, 2023, pp. 109255, https://doi.org/10.1016/j.patcog.2022.109255.

[22] J. H. Peng et al., Clustering Algorithms to Analyze Molecular Dynamics Simulation Trajectories for Complex Chemical and Biological Systems, Chinese J Chem Phys, Vol. 31, 2018, pp. 404-420, https://doi.org/10.1063/1674-0068/31/cjcp1806147.

[23] N. V. Hong, Structure and Density Heterogeneities of Silica Glass: Insight from Datamining Techniques, Silicon, 2024, https://doi.org/10.1007/s12633-024-03148-9.

[24] A. Fernández; S. Gómez, Solving Non-Uniqueness in Agglomerative Hierarchical Clustering Using Multidendrograms, Journal of Classification, Vol. 25, 2008, pp. 43-65, http://dx.doi.org/10.1007/s00357-008-9004-x.